Gamma-Ray Burst In *Swift* Era: Analysis Of Afterglow Light Curves

A THESIS SUBMITTED TO
THE SCHOOL OF GRADUATE STUDIES OF
ADDIS ABABA UNIVERSITY
IN PARTIAL FULFILLMENT OF THE
REQUIREMENTS FOR THE DEGREE OF
MASTER OF SCIENCE IN PHYSICS

BY
Deres Endalamaw Ayele

ADDIS ABABA UNIVERSITY
ADDIS ABABA, ETHIOPIA
OCTOBER, 2017

ADDIS ABABA UNIVERSITY
DEPARTMENT OF PHYSICS

The undersigned hereby certify that they have read and recommend to the Faculty of Science, School of Graduate Studies for acceptance a thesis entitled "**Gamma-Ray Burst In *Swift* Era: Analysis Of Afterglow Light Curves**" by **Deres Endalamaw Ayele** in partial fulfillment of the requirements for the degree of **Master of Science**.

Dated: October, 2017

Advisor: _____
Remudin Reshid(PhD)

Examiner: _____
Tilahun Tesfaye(PhD)

_____

ADDIS ABABA UNIVERSITY

Date: **October, 2017**

Author: **Deres Endalamaw Ayele**

Title: **Gamma-Ray Burst In *Swift* Era: Analysis Of Afterglow Light Curves**

Department: **Physics**

Degree: **M.Sc.** Convocation: **October** Year: **2017**

Permission is herewith granted to Addis Ababa University to circulate and to have copied for non-commercial purposes, at its discretion, the above title upon the request of individuals or institutions.

Signature of Author

Dedication

This work is dedicated to my family

Table of Contents

List of Tables

List of Figures

Acknowledgements

First of all, I would like to thank my advisor, Dr.Remudin Reshid, for all of his encouragement, support, devotion of his time and energy in his continuous assistance.

I would like to express my gratitude to my former advisor, Dr.legesse Wetro, for which topic of my work has been belongs to him.

I am also very grateful to Addis Ababa University, Department of Physics for this research opportunity it has provided me. I extend my thanks to staff members of physics department that they provided me many courses and thanks to Ms Tselat, secretary of the Physics department for her kindness helping.

I am also very grateful to my MSc Sponsorship, ministry of eduction of Ethiopia and regional state of Oromia.

I would also like to sincerely thank all other members of my thesis research committee, those who spent their own time and effort to reading my thesis thoroughly and provided valuable comments and suggestions.

Finally, of course, I am grateful to my wife Tigist Fikadu and my child Eldana Deres, for their help in this work and peaceful love to me.

Deres Endalamaw Ayele
Addis Ababa, Ethiopia
October, 2017.

Abstract

We presented the temporal study of all swift/XRT observations of GRB afterglows discovered between January 2005 and July 2005 which they have two or more than two breaks and well known redshift. After constructing and fitting all light curves using MATLAB programming, we have analyzed the temporal and spectral indices for each segments in the canonical X-ray afterglow light curves.

The temporal decay index is calculated using $\alpha \approx \frac{\log f_1 - \log f_2}{\log t_2 - \log t_1}$. And the numerical values, resulted from the manipulation, were mostly consistent to the theoretical temporal decay index for each GRBs in each segments. And the spectral index is from closure relation such as $\alpha = 2 + \beta$.

In our work, we have used the data of flux decay and time from the Evans et al swift/XRT online repository of United Kingdom solar system data center (UKSSDC). Once we extracted data, we have analyzed the given data to identify the behaviors of the afterglow light curves. The data, we have used, had positive and negative error approximation. Then we have analyzed the data and compared the result and the theoretical value of temporal decay index. Finally the results have been nearly confirmed to $3 \lesssim \alpha_1 \lesssim 5$ in early steep decay, the shallow decay with $0.5 \lesssim \alpha_2 \lesssim 1$, normal decay with $1.0 < \alpha_3 < 1.5$ and late steep decay α_4. $> \sim 2$.

Chapter 1

Introduction

Gamma rays are high energy electromagnetic radiation . Electromagnetic radiation actually forms a continuous spectrum, from low frequency radio wave (3 Hz) to gamma rays at $10^{18} Hz$. Gamma-rays have an energy $10^4 eV - 10^7 eV$ and wavelength less than 10^{-11} m (100 pm) [1].

Gamma-ray bursts (GRBs) are sudden, a bright/intense flashes of gamma-rays. They are the most luminous electromagnetic phenomena for a few blind seconds/a few milliseconds to hundreds of seconds in the universe. They are unpredictable in nature and distributed isotropically across the sky with equivalent luminosity of up to 10^{54} ergs^{-1} in gamma ray alone [2].

The initial prompt phase lasts typically less than 100 s and has an energy content of $\sim 10^{51}$ ergs. The initial outburst of high energy emission of GRBs is related to as the prompt phase which is accompanied by a less energetic afterglows. During the prompt gamma-ray phases, the emission is highly variable and produces light curves that frequently show multiple peaks. This emission after an initial outburst followed by a longer lasting afterglow through x-ray, optical and radio wavelength bands [3].

Before swift era, x-ray afterglow emission was detected only several hours after

burst. In such detection, the flux typically showed smooth power law decay $\sim t^{-1}$. In contrast, the optical afterglow light curves often showed an achromatic steepening decay to $\sim t^{-2}$. This was attributed to a narrow jets whose edges become visible [4].

The afterglow emission of GRBs was well described by a fireball model [5]. This model detail explained the temporal and spectral behaviors of the emission that is created by external shocks. These external shocks created when a collimated ultra relativistic jets plough into the circumstance medium [6].

The early afterglows light curves exhibit a considerable variety and rebrightenings. GRB021004 was one of the best studied events such as explaining temporal behavior, variable density profile, break frequency and jet behavior [7]. In the swift era, the early afterglow exhibited a smooth decay which was well fitted by a power law ($f_\nu \sim t^{-\alpha}$), where f_ν is the flux of the decay, α is the temporal index and t is the time of burst [8]. Swift also designed to probe exactly the density profile of the external medium and the early radiative energy losses from the external shocks. Its observational time window is from $\sim 10^2$ - 10^4 seconds after burst onset. As we have describe above, the afterglow light curves studied before and after the swift. But the detailed behaviors of the afterglow light curves was studied in swift era.

1.1 GRBs and their historical background of mission

1.1.1 Pre-swift era

GRBs were first detected in 1967 by Vela satellites. And it was named as GRB670702 (where the first number is burst year, the second number is burst month and the last number is date of the burst starting from GRB) which showed two peaks in the burst

activity over a period of seconds. However, this discovery was not published until 1973. These vela satellites detected about 70 GRB over about 10 years [9]. In the pre-swift era, there were two main detections such as Burst and Transient Source Experiment (BATSE) and BeppoSAX.

BATSE

For the next couple of decandes (1973-1991) other space based instruments contributed to increase the GRB sample size. Even this showed an isotropic distribution in the sky, it was not possible to localize GRBs in the sky to do effective follow up observations. In 1991 NASA launched a satellite equipped with capabilities to study and monitor GRBs in a systematic way. This was the Compton Gamma Ray Observatory (CGRO), which carried the (BATSE). In its 9 year lifetime BATSE detected 2704 GRBs in the 20 keV to $>$ 800 keV energy rang [10].

BATSE was that the angular distribution of GRBs on the sky appeared to completely isotropic as shown in Fig.1.1. This indicated that GRBs were most likely extragalactic in origin. Evidence shown that the weakest and brightest GRBs are isotropic [11]. This confirms that GRBs are not located in many Galaxies, but they are extragalactic events. The hint from earlier instruments was confirmed that GRBs come in two distinct classes of short and long bursts, with distributions crossing at $\sim$ 2 seconds duration [11].

BeppoSAX and the afterglow era

The next important milestone in GRB research was in 1997. After three decandes from the first detection, GRB afterglows were discorded by the Italian-Dutch satellite BeppoSAX [13]. Having been launched in 1996, BeppoSAX had the capability to

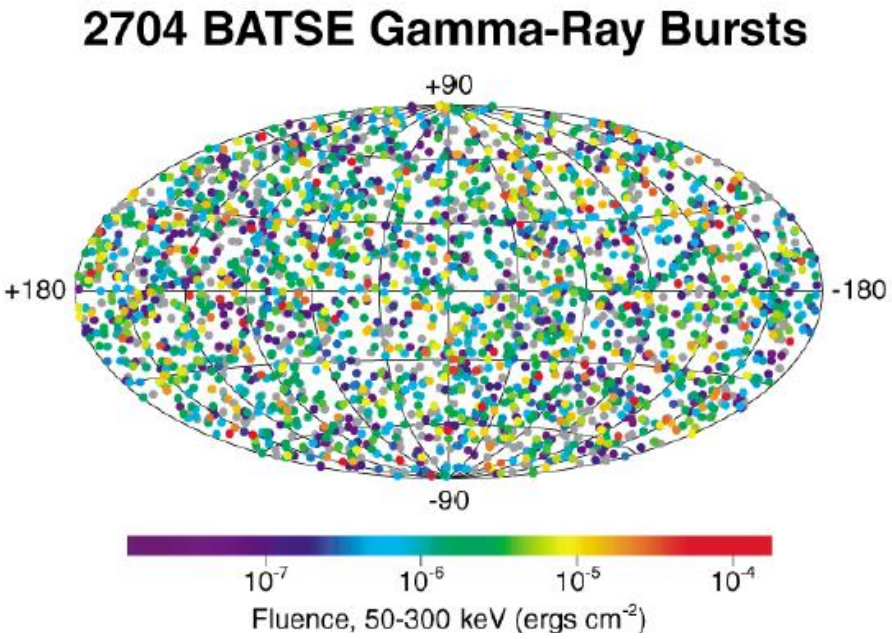

Figure 1.1: Isotropic distribution of the 2704 BATSE GRBs [12]

detect and localize GRBs. BeppoSAX had perform deep X-ray observation with in hours after burst. This made it possible to detect the first X-ray afterglow for GRB970228 with its all-sky gamma ray burst monitor (GRBM) in the 40 keV - 70 keV energy rate. This satellite has observed with its two wide field cameras (WFCs) in the energy range of 2 - 26 keV [14].

It also localized the GRB promptly with in a few arcminute accuracy. This fast imaging and arcminute localization prompted a multi-wavelength campaign. Then, this led to the identification of an afterglow in optical and radio consistent with the x-ray sources [15]. The first radio afterglow was detected GRB970508 happens during the same year [16]. This GRB970508 had a particularly bright afterglow which enabled the measurement of its spectrum. The spectrum showed a few absorption lines using them, for the first time, the redshift of GRBs was measured with the value

z= 0.835 [17].

1.1.2 Swift GRB and recent developments

Swift is a multi-wavelength space observatory which is designed to the study of GBRs. Its three instruments work together to observe GRBs and their afterglows in the gamma-ray, X-ray, ultraviolet and Optical wavebands. These instruments (see Fig. 1.3.) are burst alert telescope (BAT), X-ray telescope (XRT) and ultraviolet telescope/ optical telescope (UVOT) [18].

BAT

BAT detects GRB events and computes its coordinates in the sky. It locates the position of each events with an accuracy of 1 - 4 arcminutes with 15 seconds. This position is immediately relayed to the ground and rapid slew-ground based telescope catches the information [19].

XRT

It takes image and perform spectral analysis of the GRB afterglow. This provides more precise location of GRB with a typical error circle of approximation 2 arcseconds radius. The XRT also used to perform long term monitoring of GRB afterglow light curves. The telescope has the energy range of 0.2 keV - 10 keV [20].

UVOT

UVOT used to detect optical afterglow and provide a sub-arcseconds position. UVOT provide optical and ultraviolet photometry through filters and law resolution spectra (170 - 650 nm) through the use of optical and UV grisons. It is also used to provide long-term follow ups of GRB afterglow light curves [21]

Mission history of swift

The Swift Gamma-Ray Burst Mission consists of a robotic spacecraft called Swift, which was launched into orbit on November 20, 2004 [22]. It orbits at 567 km x 585 km with a period of $\sim$ 95.9 min. Swift is the first multi-wavelength mission for the study of GRBs, being elaborated by an international collaboration.

May 9, 2005, swift detected GRB050509B, in which a burst of gamma rays that lasted one-twentieth of a second. The detection marked the first time that the accurate location of a short duration GRB [23]. In the later years, swift detected many GRBs per month such as by 2010, swift had detected more than 500 GRBs [24], by October 2013 more than 800 GRBs [25] and by October 27, 2015 more than 1000 GRBs [26].

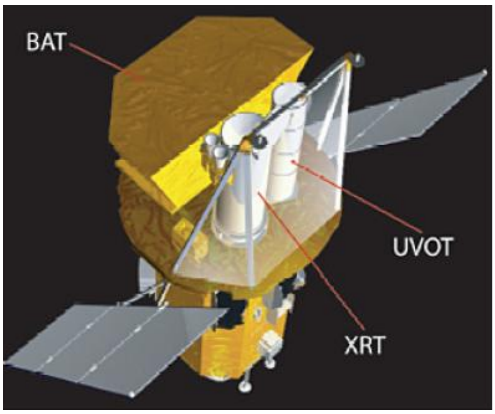

Figure 1.2: Swift satellite of NASA

The general characteristics of swift mission is given in table 1.1.

Table 1.1: characteristics of swift mission

mission parametrs	values
slew rate	50^o in less than 75 s
orbit	low earth, 600 km altitude
Inclination	22^o
Launch vehicle	Delta 7320-10 with 3m fairing
Mass	1450 Kg
power	1040 W
Launch date	November 20,2004

1.2 Burst types and classes

Based on their duration and hardness ratio, GRBs has been grouped into short/hard and long/soft GRBs.

1.2.1 Short/hard GRBs

The burst events with a duration less than about 2 seconds are short/hard GRBs. Until 2005, there were no short afterglows had been successfully detected. They have more highly energetic /hard gamma-rays than their long burst counterparts. In this burst, the conversion of energy into gamma- rays decreases as the burst progresses. For short GRBs, the T_{90} (90% of the fluency is detected), as shown in (Fig. 1.3.), has been less than 2 seconds [27]. There is no radio, optical, or x-ray counterpart has found for any short burst [28]. Short duration bursts counts 30% of the GRBs in any burst.

1.2.2 Long/soft GRBs

The GRBs which is the most observed (70%) and have a duration of greater than 2 seconds are long/soft GRBs. All long bursts display X-ray afterglow and only about

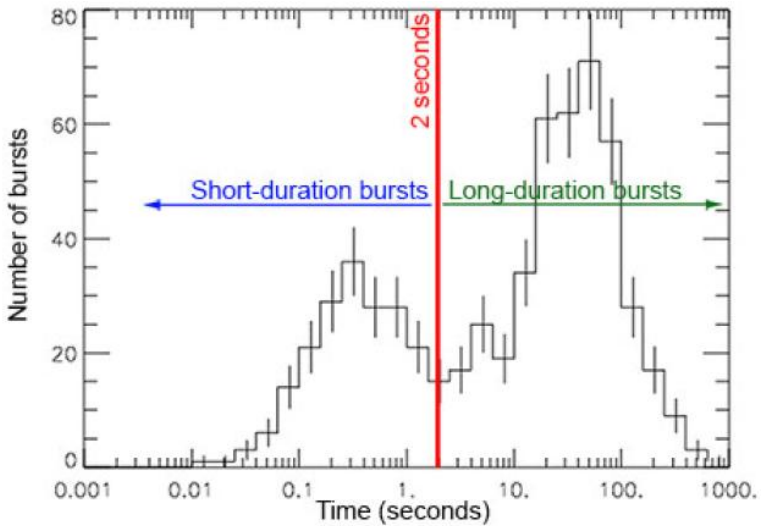

Figure 1.3: Duration of distribution for 222 BATSE GRBs. [27]

one-half of them have detectable radio or optical afterglows. As we have shown in (Fig. 1.2.), long duration bursts have T_{90} which is grater than 2 seconds. The energy conversion of this type of burst appears to remain constant throughout the burst[29].

Generally gamma-ray bursts have been detected with different instruments. However, there is no perfect instrument as swift in determination of prompt and afterglow emission. Swift mission has detected the temporal behaviors of most GRBs. GRBs afterglow light curves specially the X-ray light curves have been analyzed in this thesis.

There are multiple questions regarding to our work. Among these questions

(1) Did the temporal index values of any random GRBs confirm to the values proposed in different times within XRT canonical light curves?

(2) Could some of the breaks at the end of the plateau phases actually be jet break or late steep decay phase?

(3) Could the spectral index obtained from the closure relation in initial steep decay phase confirm to the theoretical limit? The goal of this thesis was attempt to answer these questions.

1.3 Layout of the thesis

In this review, we described the stages of the gamma-ray bursts i.e the historical background and their types. In section two, the gamma-ray burst emission mechanisms and the theoretical explanations of GRB afterglow light curves are discussed. The methodology of numerical analyzing is discussed in section three. Analyzing the selected GRBs' afterglow light curves and the conclusion of the result are discussed in section four and five respectively.

Chapter 2

GRB emission mechanism

Introduction

GRB emission mechanisms are the theories or models that explain how the energy from GRBs progenitor is turned into radiation. In this section of the thesis, we discussed the fireball model, in which we explain the way of gamma-ray production. The mechanisms of the GRB emissions that are prompt and afterglow emissions and afterglow light curves are discussed in detail.

Fireball model

Fireball model is the standard model for explanation of GRBs. The mechanisms of fireball model starts the understanding of the production of prompt and afterglow from GRBs [30]. This model provides a key episodes of energy conversions in GRBs.

Initially, as we have shown in (Fig.2.1.), a large amount of gravitational energy $\sim 10^{53}$ erg or more is released in a very short time into the compact region. Due to the source of this energy, the collapse of the massive stars (merger of two neutron stars or neutron stars and black holes) is created. And then a part of this kinetic energy is used to produce a relativistic jets. This is the stage in which GRB jets are produced [31].

Once the GRB jets are formed, they accelerated to the relativistic velocities. As we have observed in (Fig.2.1), at radius r = 10^{11} cm from the compact region, the thermal photons decouple at the photosphere. A part of the jets' kinetic energy is dissipated by internal collisions/shocks and produced gamma-rays that we observed in the prompt emission. The remaining kinetic energy of the relativistic jets runs into interstellar medium (ISM) and heats it. Then it produced the observed afterglow. Finally the kinetic energy is gradually converted to heat and the afterglow gradually fades [31].

2.1 Prompt emission

It is believed to be generated by internal shocks within the fireball that rise above the pair production photosphere at $\sim 10^{12} - 10^{14}$ cm. These shocks stem from mini-shells within a jet produced by unsteady accretion of material onto black hole or by the merger of neutron star to neutron star [32]. The shells have a distribution in lorentz

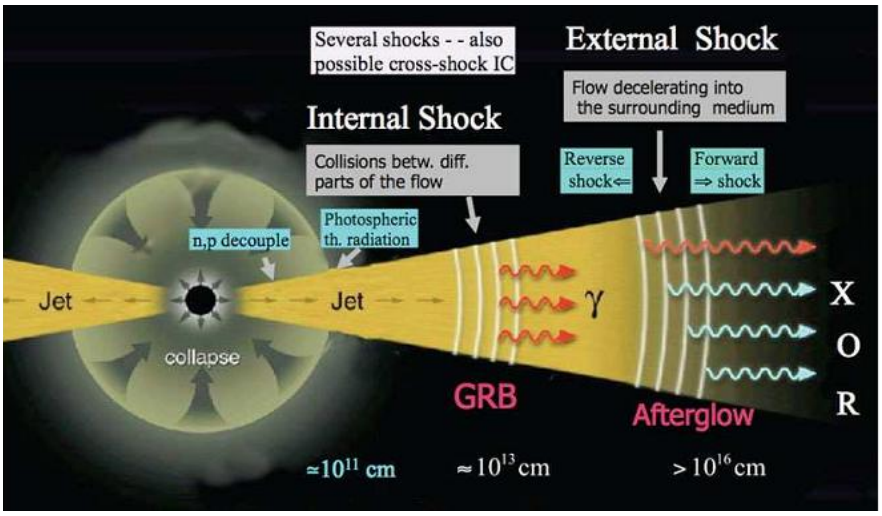

Figure 2.1: A schematic model of the fireball model of GRBs [34].

factor γ, in which $\Delta\gamma \propto \Gamma$ where Γ is bulk lorentz factor. In the region around $\sim 10^{12} - 10^{14}$ cm (see Fig. 2.1.), the collisions between different parts of the flow is produced in different shells. As a fast shell catch up with a slower ones, they form strong internal shocks that propagates in both shells. Once above the photosphere, the heated and accelerated electrons cool by synchrotron emission [33].

This radiation is observed in γ-ray band. Each collision that occurs above pair photosphere produces a pulse in the GRB's light curves [34].

2.1.1 Internal shocks

Internal shock is the collision of multiple shells traveling with different velocities in the photosphere region. The collision of two thin shells heat the matter. Due to this enormous amount of energy converted into kinetic energy and produced the γ-ray emission [35].

The efficiency of internal shocks is determined by the ratio of lorentz factor of the colliding shells. If the the lorentz factor ratio (γ_2/γ_1) are allowed, the internal shock efficiency is limited by the fraction of energy in radiating electron [36]. Multiple collisions between shocks may also result in ultra efficient internal shocks for radiating electron away [37].

2.1.2 External shock

A relativistic materials/jets are running into some external ambient medium i.e interstellar medium or stellar wind. In each time, the ejecta run a high density environment in which they produced a peak in the mission called external shock [38]. In the external shocks, the jets may be forward shocked or reverse shocked.

As the material in the jet expands, accelerates and compresses interstellar medium,

it creates a forward shocks. The deceleration of forward shocks is occurred when the rest mass energy of the swept up particles equal to the ejected energy. This sets a deceleration length scale at ($\sim 10^{16}$ cm) [38]. The reverse shock is formed by the deceleration of the jet material and propagates back into the relativistic flow. This happens when the rest mass energy of the swept up particles is greater than the ejected energy [38].

2.2 Afterglow emission

Afterglow emission is the emission in which, the slowly fading emission of initial GRB at longer wavelength after GRB. This emission is created by the collision between the burst eject and interstellar gas. The GRB itself is rapid, lasting from less than a second up to a few minute at most. Once it disappears, it leaves behind a counterpart at a longer wavelength (X-ray,Uv/Optical and radio bands) [39]. Then, they are generally remain detectable for days or longer. As we have described above, afterglow emissions are dominated by external shocks.

The early searches were unsuccessful largely because it was difficult to observe the bursts' position at a longer wavelength immediately after the initial burst. The break through came in February 1997 when the satellite BeppoSAx detected a GRB970228. The William Herschel telescope identified an optical counterpart 20 hours after burst. Once the GRB faded deep imaging was able to identify a faint, distance host of galaxy at a location of GRB as pinpointed by the optical afterglow [40].

2.3 Afterglow observations and interpretation

2.3.1 Late time afterglow observation and interpretation

Before swift mission, afterglow observations was started after several hours ($\gtrsim$ 10 hrs) after bursts trigger. The optical afterglow of late time afterglow displays a power law decay behavior $F_\nu \propto t^{-\alpha}$, with a decay index $\alpha \sim 1$ [41]. The temporal break in the optical afterglow light curve was detected for bright GRBs. The break time is typically around a day and followed by the steeper decay with decay slope of $\alpha \sim 2$ [42].

The radio afterglow light curve initially rises and reaches a peak around 10 days after which starts to decline [43]. The peak usually corresponds to the passage of synchrotron injection frequency ν_m or synchrotron self absorption frequency ν_a through the radio band. The broad band afterglow spectrum can be fit with a broken power law at a fixed observer time [44].

2.3.2 Theoretical interpretation of the X-ray afterglow light curves in swift era

The detection of GRBs early afterglows is within less than 100 seconds after trigger in the swift mission. The canonical X-ray afterglow light curves generally concludes four phases such as early time steep decay phase, the shallow decay phase/plateau phase, normal decay phase and late steep decay phase [45].

Steep decay of early X-ray light curves

This phase is the tail of prompt emission. This phase is also governed by curvature effect, for which emission from different viewing angles reaches the observer with different delays due to the light propagation effects [45]. The relationship between

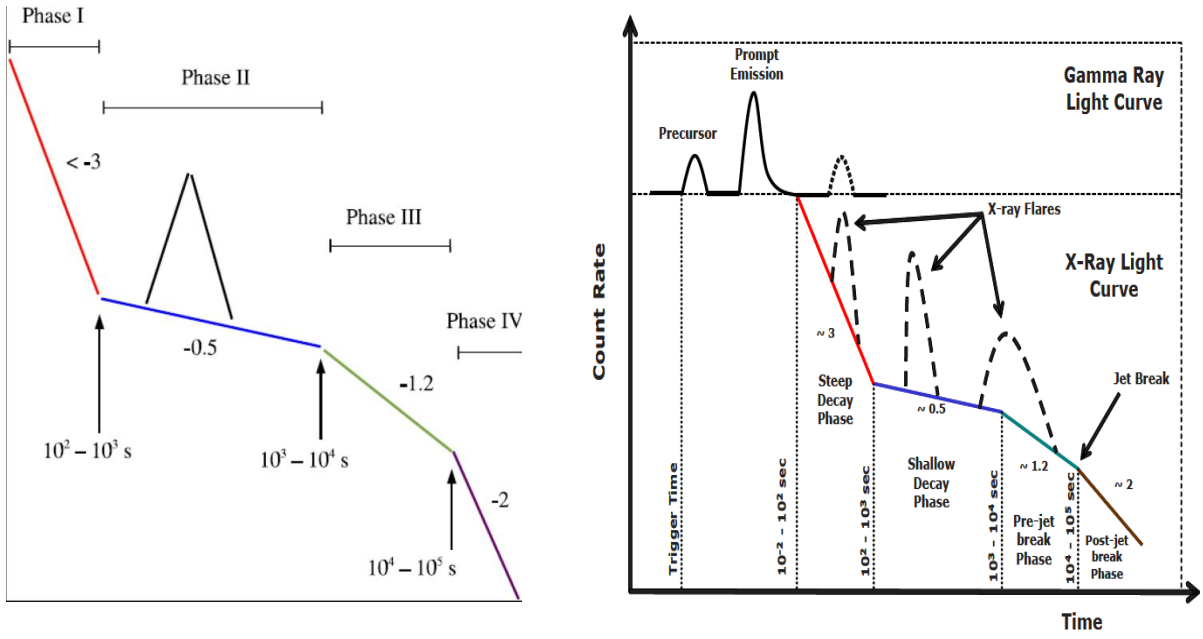

Figure 2.2: Canonical GRB afterglow light curves [46].

temporal and spectral slopes of higher latitude emission is $\alpha = 2+\beta$. It is independent of any of the environmental or other parameters such as peak frequency and cooling frequency that affects the closure relations for the external shocks.

Swift answer the debate of separation between the prompt emission and late afterglow regarding to internal and external origin of the prompt emission i.e internal shocks are the origin of prompt emission [47]. As it has shown in (Fig. 2.2.), early steep decay slope is around $3 < \alpha_1 < 5$.

This phase may be simply the high latitude emission associated with the prompt gamma-ray sources at R $\gtrsim 10^{15}$ cm when the central engine turns off faster than the decline of the X-ray light curves [48]. On the other hand, if the emission region is at much smaller radius than the rapidly declining X-ray light curve reflects the time

dependence of central engine activity [49].

Detailed analysis of a sample of GRBs suggests that the high latitude "curvature effect" model can explain the early steep decay phase [50]. As we have shown in (Fig. 2.3.), the achromatic change of phases for sample GRBs indicates the light curves transition. These GRBs followed the decay power law relation $F_\nu \propto t^{-\alpha_1}$ where, $\alpha_1 = 2 + \beta$ for curvature effect model. Generally, this phase has already stayed between the time interval of $10^{-2} - 10^2$ seconds and $10^2 - 10^3$ seconds which is presented in (Fig. 2.2.) in the right side.

Shallow decay X-ray light curves

This phase is sometimes called plateau phase and very small decay with value of decay $0.5 < \alpha_2 < 1.0$. This phase rises when the energy ejected to the decelerated external shock. When the energy is terminated, the decay of light curves become slow down and the transition to phase three (normal decay) is occurred [51]. In this phase, the shape of light curves in the X-ray and optical bands should be similar where break occur at the same time in these bands [52].

There are two acceptable explanations behind the emission mechanisms of this phase. (1) A smooth and gradual energy injection that arrives in the forward shock, is due to the decrease of the lorentz factor Γ at the end of prompt emission. The mass that is injected to the forward shock is the function of its lorentz factor and the energy injected. As a result Γ increases monotonically with radius,(which we discussed in detail in section (2.4.)). The flux decays are a power law and depends on the mass and the energy injected [53]. (2) The central engine of the source stays active for hours after the burst and injects the smooth and continues energy at later times, several times after the burst [54].

X-ray plateaus results from the contribution of prompt X-ray emission scattered by dust in the host galaxy. The optical flux or the powerful outburst episode is already ruled out by the prompt optical data [55].

Normal decay phase

This is the third phase in this canonical phase description. This phase has a decay slope around $1.0 < \alpha < 1.5$ which was expected before swift and it is consistent standard fireball afterglow model in ISM [56]. The explanation of this phase is related to the end of energy injection at the external shocks.

This implies (1) the fall of the lorentz factor of forward shock up to the point of minimal lorentz factor that carries a significant initial energy. (2) The time that the central engine needs to be in active [57]. In general the normal decay is expected in the standard forward shock.

Late steep decay following the plateau in X-ray light curves

In this phase (IV) in (Fig. 2.2.) left side, the decay slope is greater than 2. After the normal decay, X-ray emission is powered by a continues jet from a long lasting central engine. Then X-ray flux from the external shock is buried beneath this emission [58]. Indeed, the canonical X-ray light curve can be matched with the accretion history in the collapsar GRB model. This model assume that the X-ray luminosity is proportional to the accretion power of the central engine [59].

This late steep decay of swift, represents an achromatic steepening that happens due to the jet breaks. When the lorentz factor of the ejecta becomes larger than θ_0^{-1} compared to the jet opening angle θ_0, the ejecta is collimated into a jet break. Finally, this phase is expected in the forward shock model as a jet break. Jet breaks

are thought to happen due to the beaming of the emission from GRBs. This phase has pre-jet-break phase and post-jet-break phase, (see in Fig. 2.2.).

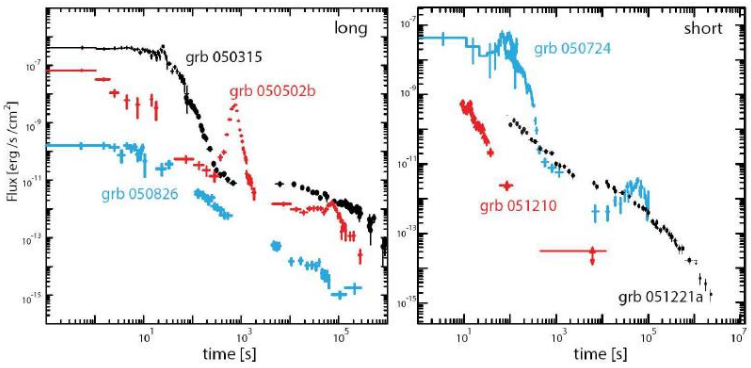

Figure 2.3: Examples of GRBs X-ray afterglow light curves for both long and short bursts

2.3.3 Time of breaks in swift afterglow light curves

In (Fig. 2.2.), there are three break points and the time at that points are called breaking time of afterglow light curves. These break times are the first break time, the second break time and the jet break time.

The first break in the light curve ($t_{break,1}$)

This is the time at which the phase change of light curves from phase I to phase II is took places. As we have shown in (Fig. 2.2.), the $t_{break,1}$ is around $t_{break,1}$ $(10^2 - 10^3)$ seconds $< t_1 < t_{break,2}$ $(10^3 - 10^4$ seconds).

The first break time is also the time when the slow decaying emission from the forward shock become dominant over the rapidly decaying flux from the prompt emission at a large angle. In sharply decaying flux, the prompt emission initially dominates over the external shocks at $t > t_{break,1}$ [60].

2.4 Flux decay with time of observed light curve

When relativistic, conical and optically thin source moving with a lorentz factor Γ turns off abruptly, the flux declines rapidly with time [61]. In such type of source which is specified with spherical co-ordinate (r,θ, ϕ), the source turned off at $r = R_0$. where r is the radius of the photo/jets, R_0 is the radius of the observer and θ is measured with respect to the line of sight to the observer.

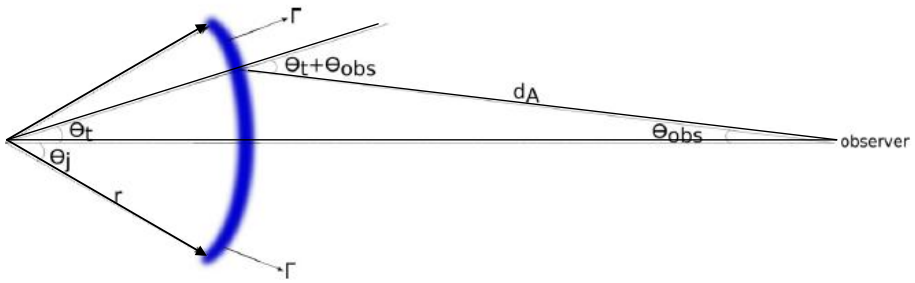

Figure 2.4: High latitude emission when the gamma-ray source turns off suddenly

The time dependence of observed flux follows from the lorentz transformation of specific intensity. The specific flux in the observer frame from the relativistic source of moving object with specific intensity $I'_{\nu'}$ and spectrum frequency $\propto \nu'^{-\beta}$ is given by

$$f_\nu(t_{obs}) = \int d\Omega_{obs} I_\nu cos\theta_{obs} \tag{2.4.1}$$

where $d\Omega_{obs}$ is the solid angle of the source, I_ν is the specific intensity of the source photon. To derive the standard flux decay of GRBs, let we define $d\Omega_{obs}$ and I_ν in the relativistic beaming.

In relativistic beam of photons, the transverse component of the momentum does not change under lorentz transformation, i.e. its comoving and lab frame values are

the same. Thus

$$\nu sin\theta = \nu' sin\theta' \tag{2.4.2}$$

or

$$sin\theta = (\nu'/\nu) sin\theta' \tag{2.4.3}$$

Since the photon frequency on the observer frame, ν, can be expressed in terms of the comoving frequency, ν', using standard lorentz transformation of photon as

$$\nu = \frac{\nu'}{\Gamma(1 - vcos\theta/c)} = \nu' D \tag{2.4.4}$$

where D is standard doppler effect which is expressed as $[\Gamma(1 - vcos\theta/c)]^{-1}$. Then the ratio of the frequency become $\nu'/\nu = 1/D$ and substituting this ratio into Eq. (2.4.3), we obtain

$$sin\theta = \frac{sin\theta'}{D} \tag{2.4.5}$$

For large Γ, $\theta \approx \theta'/\Gamma$. This tells us photons are focused in the forward direction such that the angular size of photo beam in the lab frame is smaller than it is in the comoving frame by a factor $\sim \Gamma$. And also the solid angle for a canonical beam of photons in lab frame is smaller than in the comoving frame by a factor of $\sim \Gamma^2$. This implies the lorentz transformation of solid angle is

$$d\Omega = sin\theta d\theta d\phi = \frac{sin\theta' d\theta' d\phi'}{D^2} = \frac{d\Omega'}{D^2} \tag{2.4.6}$$

The other parameter in the lorentz transformation is the specific intensity. It is defined as flux per unit frequency and solid angle carried by photos traveling with in a narrow conical beam with its axis perpendicular to surface dA. This means

$$I_\nu \equiv \frac{dE}{d\nu dt_{obs} dA d\Omega} \tag{2.4.7}$$

Considering $d\nu' dt'_{obs} dA' = d\nu dt_{obs} dA$, are lorentz invariants and using Eq. (2.4.6) and $E = \Gamma E'$, Eq. (2.4.7) can be reduced to

$$I_\nu = D^3 I'_{\nu'} \tag{2.4.8}$$

Since for intrinsic spectrum, $I'_{\nu'} = I'\nu'^{-\beta}$,where β is spectral index, then the specific intensity is summarized as

$$I_\nu = D^3 \nu'^{-\beta} I' \tag{2.4.9}$$

This equation, can be simplify by substituting the value of ν' from the Eq. (2.4.4).

$$I_\nu = D^{3+\beta} \nu^{-\beta} I' \tag{2.4.10}$$

Finally substituting Eq. (2.4.6) and Eq. (2.4.10) into Eq. (2.4.1) and integrating over $d\phi$ in the interval $0 - 2\pi$, the observed flux becomes

$$f_\nu(t_{obs}) = 2\pi \int d\theta_{obs} \frac{I'_{\nu'} \nu'^{\beta}_0 sin2\theta_{obs} [(1+z)\Gamma]^{-(3+\beta)}}{2\nu^\beta (1 - vcos(\theta + \theta_{obs})/c)^{3+\beta}} \tag{2.4.11}$$

where ν'_0 is the frequency that lies on the power law segment of the spectrum for $I'_{\nu'}$. Using the law of sine from the diagram in Fig. 2.4, we see that $\frac{sin\theta}{d_A} = \frac{sin\theta_{obs}}{R_0}$, this implies $sin\theta_{obs} = \frac{R_0}{d_A} sin\theta$ and substituting into Eq. (2.4.11) ,in the case $\theta_{obs} \ll \theta$, yields

$$f_\nu(t_{obs}) = \frac{2\pi I'_0 \nu'^{\beta}_0 \nu^{-\beta}}{[(1+z)\Gamma]^{3+\beta}} (\frac{R_0}{d_A})^2 \int_{\theta_t}^{\pi/2} d\theta \frac{sin\theta cos\theta}{(1 - vcos\theta/c)^{3+\beta}} \tag{2.4.12}$$

Using substitution method of integrating, this equation can be simplified as

$$f_\nu(t_{obs}) \propto (1 - vcos\theta_t/c)^{-(2+\beta)} \nu^{-\beta} \tag{2.4.13}$$

Photons released at (r= vt, θ, ϕ) arrive at the observer frame with a time delayed to a photon emitted at r = 0 of

$$t_{obs} = t - rcos\theta/c = t(1 - vcos\theta/c) = t/\Gamma D \tag{2.4.14}$$

From this equation, the relation between t_{obs} and D is $t_{obs} \propto D^{-1}$. Then the flux decay with time of the observed light curves from Eq. (2.4.13) is summarized as

$$f_\nu(t_{obs}) \propto t^{-(2+\beta)}\nu^{-\beta} \tag{2.4.15}$$

The standard convection of flux decay is

$$f_\nu(t_{obs}) \propto t^{-\alpha}\nu^{-\beta} \tag{2.4.16}$$

where $\alpha = 2 + \beta$.

2.5 Estimating the gamma-ray luminosity

Luminosity is the amount of electromagnetic energy a body radiates per unit of time. The observed isotropic-equivalent luminosity in the X-ray afterglow ,L_X can generally be expressed as

$$L_X(t) = \int_{\nu_1}^{\nu_2} L_\nu(t)d\nu \tag{2.5.1}$$

since $\mathrm{L}_\nu(\mathrm{t}) = 4\pi\ \mathrm{d}_L^2\mathrm{F}/(1+\mathrm{z})$, substituting $\mathrm{L}_\nu(\mathrm{t})$ into Equ. (2.5.1) yields

$$L_X(t) = \frac{4\pi d_L^2}{(1+z)} \int_{\nu_1}^{\nu_2} F_\nu/(1+z)[(1+z)t]d\nu \tag{2.5.2}$$

where d_L is the luminosity distance, ν_1 and ν_2 are the spectral frequencies in the energy band, z is the redshift and $L_\nu(t)$ is the spectral luminosity at the cosmological frame of the source, i.e, both ν and t are $L_\nu(t)$ are measured in the frame [62].

$$L_X(t) = 4\pi d_L^2 \int_{\nu_1/(1+z)}^{\nu_2/(1+z)} F_\nu[(1+z)t]d\nu \tag{2.5.3}$$

since $F_\nu(t)$ is measured in the observer frame and assumed in standard form, Eq. (2.5.3) can be reduced to:

$$L_x(t) = 4\pi d_L^2 (1+z)^{(\beta-\alpha-1)} F_x(t) \tag{2.5.4}$$

Where $F_x(t) = \int_{\nu_1}^{\nu_2} F_\nu(t)$.

In summary, swift observation have led to the better understanding of afterglow light curves for the initial few hours. The two mechanisms of emission have related to the central engine of the burst. The four phases of the afterglow light curves are clearly captured with swift. Finally we have understand that the flux decay of afterglow light curves are governed with standard law of decay, i.e $f_\nu(t_{obs}) \propto t^{-\alpha}\nu^{-\beta}$,where $\alpha = 2+\beta$.

This is a theoretical understanding for the afterglow era. Let we introduce the methodology of analyzing the temporal and spectral analysis of the afterglow in the next section.

Chapter 3

Methodology

Introduction

In this section, we have described the method that were used in this thesis. The afterglow light curves were analyzed by different researcher in different times in the swift era. So that in this thesis, to understand the temporal and spectral decay indices, the following directive methods are used.

3.1 Model

We have assumed the fireball model. In standard fireball model, the behavior of X-ray light curves is assumed to be a single power law decay where flux goes as:

$$f_\nu(t) \propto t^{-\alpha} \tag{3.1.1}$$

where α is the temporal index/decay slope and $\alpha = 1, 2, 3, 4$ for early steep decay slope, shallow decay slope, normal decay slope and late decay slope respectively.

This model also indicated the closure relation of temporal and spectral indices. As we have discussed in section (2.4), in standard fireball model, we have $\alpha = 2 + \beta$.

3.2 Sample selection

In our synthesis of swift XRT light curves, GRBs have been selected in which they have more than two light curve breaks and specific or known redshift. From the Evans et al online repository, we have considered GRB data taken over the period of six month in this work, which were triggered from January 2005 - July 2005. Among 40 GRBs that were triggered during this period, we have chosen a representative sample of 4 GRBs for our analysis. The selection criterions were number of light curve breaks and known redshift.

3.3 Data analysis

The graphical relation between afterglow flux and time has been shown by using MATLAB programming for the selected data. Hereafter considering high latitude radiation and the flux decay closure relations, we made a numerical determinations of temporal and spectral indices of the afterglow decay for early steep decay and temporal index for the rest phases. In our numerical calculations, from $F_\nu(t) \propto \nu^{-\beta} t^{-\alpha}$ the flux density or flux per unit frequency was approximated to $F_\nu(t) \approx t^{-\alpha}$. Finally, we have found the values of temporal flux decay α as:

$$\alpha \approx -\frac{logf_2 - logf_1}{logt_2 - logt_1} \tag{3.3.1}$$

and the corresponding spectral index from $\alpha = 2 + \beta$.

In general, we have discussed our results whether they confirm to the earlier values by taking different approximations.

Chapter 4

Analysis of GRBs' afterglow light curves

Introduction

In this chapter we discussed the characteristics of temporal parameter of sample GRBs in four phase. The X-ray light curves are typically composed of several components in which the canonical shape has four power law segments expressed in section (2.3). The temporal parameters or the decay slope of each four phases are discussed bellow.

4.1 Swift/XRT light curve data

For our samples of GRBs on Evans et al online repository [63-64], we have the following swift/XRT data of selected GRBs. In table (4.1) and (4.2) bellow, time since BAT triggers (s) and flux through energy band (0.3 - 10 KeV)(ergcm$^{-2}s^{-1}$) have been taken randomly from the respective phases in each GRBs. These flux and time values have been selected in each phase to find the respective temporal index.

GRBs	phase I $[t(s), f(ergcm^{-2}s^{-1})]$	phase II $[t(s), f(ergcm^{-2}s^{-1})]$
050315	$t_1 = 85.86^{+2.71}_{-2.31}$	$t_1 = 11568.3^{+36.64}_{-61.14}$
	$f_1 = 8.67 \times 10^{-9} \pm 1.1 \times 10^{-9}$	$f_1 = 7.89 \times 10^{-12} \pm 1.78 \times 10^{-12}$
	$t_2 = 95.97^{+2.6}_{-2.4}$	$t_2 = 12697.85^{+57.96}_{-44.8}$
	$f_2 = 6.01 \times 10^{-9} \pm 8.9 \times 10^{-10}$	$f_2 = 7.5 \times 10^{-12} \pm 1.68 \times 10^{-12}$
050505	$t_1 = 2886.95^{+41.29}_{-53.99}$	$t_1 = 8680.73^{+26.47}_{-21.17}$
	$f_1 = 2.57 \times 10^{-11} \pm 5.7 \times 10^{-12}$	$f_1 = 1.5 \times 10^{-11} \pm 3.4 \times 10^{-12}$
	$t_2 = 3498.96^{+73.66}_{-84.3}$	$t_2 = 15333.33^{+38.12}_{-37.1}$
	$f_2 = 1.6 \times 10^{-11} \pm 3.4 \times 10^{-12}$	$f_2 = 9.67 \times 10^{-12} \pm 2.2 \times 10^{-12}$
050724	$t_1 = 79.56^{+0.4}_{-0.32}$	$t_1 = 131.85^{+0.41}_{-0.31}$
	$f_1 = 8.36 \times 10^{-9} \pm 1.04 \times 10^{-9}$	$f_1 = 4.34 \times 10^{-9} \pm 5.34 \times 10^{-10}$
	$t_2 = 84.14^{+0.49}_{-0.54}$	$t_2 = 135.52^{+0.29}_{-0.24}$
	$f_2 = 5.94 \times 10^{-9} \pm 7.8 \times 10^{-10}$	$f_2 = 4.3 \times 10^{-9} \pm 6.2 \times 10^{-10}$
050730	$t_1 = 140.24^{+0.69}_{-0.56}$	$t_1 = 261.79^{+1.66}_{-1.45}$
	$f_1 = 1.66 \times 10^{-9} \pm 2.49 \times 10^{-10}$	$f_1 = 9.3 \times 10^{-10} \pm 1.39 \times 10^{-10}$
	$t_2 = 198.39^{+1.67}_{-1.68}$	$t_2 = 770.45^{+1.96}_{-1.71}$
	$f_2 = 6.13 \times 10^{-10} \pm 9.15 \times 10^{-11}$	$f_2 = 5.55 \times 10^{-10} \pm 8.3 \times 10^{-11}$

Table 4.1: Data from Evans et al 2009 online repository for phase I and II

GRBs	phase III $[t(s), f(ergcm^{-2}s^{-1})]$	phase IV [t(s),f(ergcm^{-2}s^{-1}]
050315	$t_1 = 168320.29^{+223.78}_{-214.99}$	-
	$f_1 = 1.39 \times 10^{-12} \pm 3.64 \times 10^{-13}$	-
	$t_2 = 888451.76^{+59869.16}_{-13452.99}$	-
	$f_2 = 6.45 \times 10^{-14} \pm 2.01 \times 10^{-14}$	-
050505	$t_1 = 44079.52^{+110.35}_{-84.83}$	-
	$f_1 = 2.87 \times 10^{-12} \pm 7.48 \times 10^{-13}$	-
	$t_2 = 91151.33^{+1032.9}_{-877.36}$	
	$f_2 = 5.02 \times 10^{-13} \pm 1.06 \times 10^{-13}$	-
050724	$t_1 = 300.07^{+2.7}_{-2.27}$	$t_1 = 103776.11^{+25813.3}_{-10938.9}$
	$f_1 = 2.86 \times 10^{-10} \pm 5.22 \times 10^{-11}$	$f_1 = 2.46 \times 10^{-13} \pm 6.58 \times 10^{-14}$
	$t_2 = 316.06^{+2.9}_{-2.4}$	$t_2 = 106925.01^{+72824.49}_{-27539.37}$
	$f_2 = 2.65 \times 10^{-10} \pm 4.9 \times 10^{-11}$	$f_2 = 9.1 \times 10^{-14} \pm 1.89 \times 10^{-14}$
050730	$t_1 = 6501.9^{+13.67}_{-16.4}$	$t_1 = 10382.15^{+12.48}_{-12.59}$
	$f_1 = 1.32 \times 10^{-10} \pm 2.97 \times 10^{-11}$	$f_1 = 1.34 \times 10^{-10} \pm 2.92 \times 10^{-11}$
	$t_2 = 9954.96^{+23.5}_{-19.2}$	$t_2 = 142736.21^{+77859.3}_{-11519.61}$
	$f_2 = 7.5 \times 10^{-11} \pm 1.7 \times 10^{-11}$	$f_2 = 1.4 \times 10^{-13} \pm 3.13 \times 10^{-14}$

Table 4.2: Data from Evans et al 2009 online repository for phase III and IV

The time since BAT triggers with their respective light breaks and the flux in the swift XRT during their burst is also presented below (Fig. 4.1 - Fig. 4.4).

4.2 Result and discussion

As we have described in section (3.2), all the necessary data were from Evans et al online repository. The afterglow flux for each GRBs in the energy band 0.3 - 10 keV has been triggered in different time interval. The swift/XRT has shown all parameters for each GRBs.

For GRB050315, the swift/XRT has shown two breaking time in the decaying processes. This GRB has also three phases such as early steep decay, shallow decay and late steep decay. The values of the breaking times were $T_{break,1} = 5420^{+3570}_{-3952}$ s and $T_{break,2} = 16800^{+2900}_{-2100}$ s. Based on the data extracted from the online repository, the graphical representation of flux in the given energy band against the time of burst is drawn using MATLAB programming and presented in Fig. (4.1).

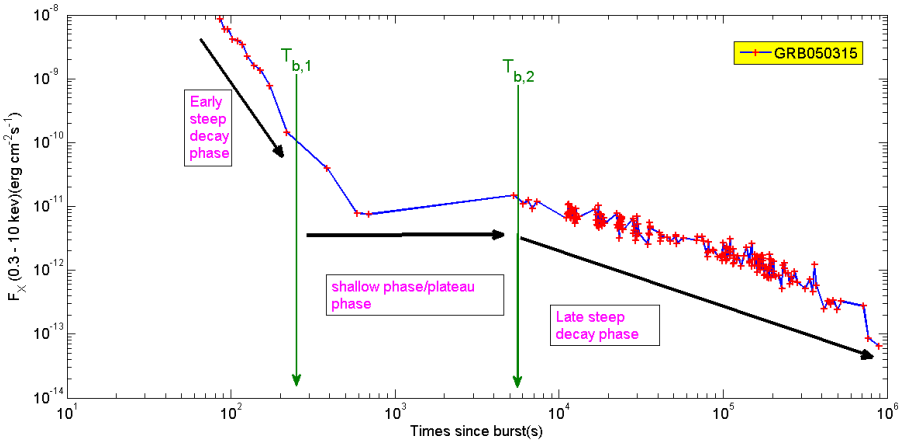

Figure 4.1: The X-ray flux (0.3 - 10 keV in the observer frame) as a function of the observed time

The data of GRB050505 was also similar to GRB050315 in case of breaking points. GRB050505 has two break times. These were the indicators for the three phases. These breaking times were $T_{break,1} = 7063^{+7060}_{-1273}$ s and $T_{break,2} = 43900^{+13600}_{-5500}$. Using the same programme, we got flux against time diagram as shown in Fig. (4.2).

However, GRB050724 and GRB050630 had three breaking time. This indicated that they had four phases of afterglow light curves. The breaking times of GRB050724 were $T_{break,1} = 132^{+4}_{-4}$, $T_{break,2} = 297^{+19}_{-103}$ s and $T_{break,3} = 472^{+40}_{-22}$ s. The phases of GRB050724 were indicated using the Evans et al data and MATLAB programming

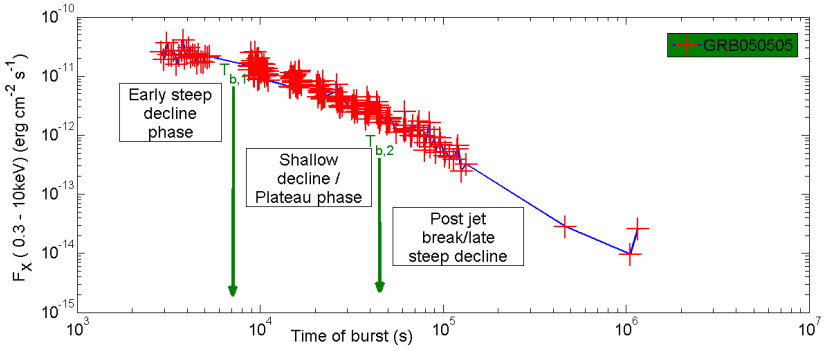

Figure 4.2: The X-ray flux (0.3 - 10 keV in the observer frame) as a function of the observed time

and and presented in Fig. (4.3).

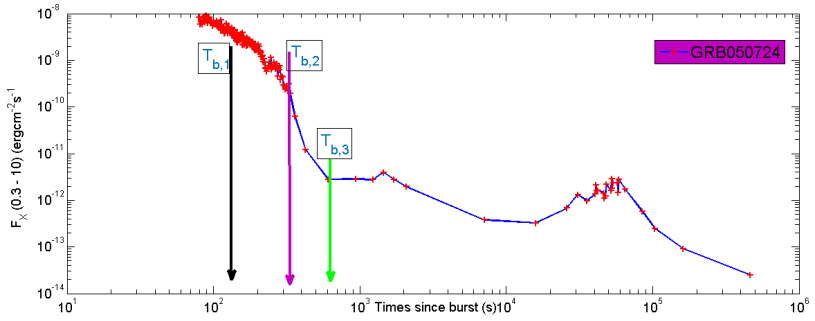

Figure 4.3: The X-ray flux (0.3 - 10 keV in the observer frame) as a function of the observed time

And finally the break time for GRB050730 has been given as $T_{break,1} = 259^{+21}_{-17}$ s , $T_{break,2} = 1832^{+397}_{-328}$ s and $T_{break,3} = 10400^{+400}_{-500}$ s. The decay that represents the afterglow light curves has been drawn using the MATLAB program and presented in Fig. (4.4).

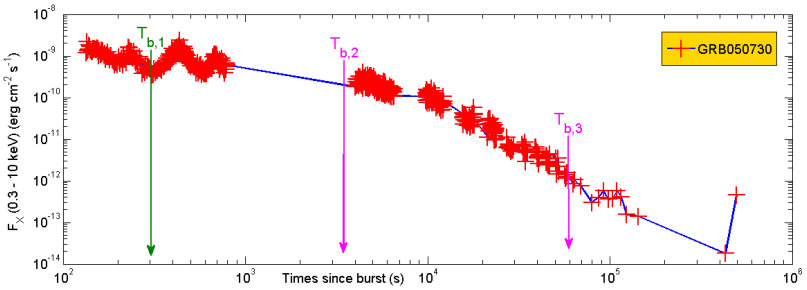

Figure 4.4: The X-ray flux (0.3 - 10 keV in the observer frame) as a function of the observed time

4.2.1 Numerical analysis of temporal indices in phase I

Based on the data in table (4.2), the temporal index early steep decay slope of each GRB was calculated. Since that data have positive and negative error measurement, the decay slope also has the error reading. As we have discussed in section (2.4), the flux decay with time for the observed light curves were summarized as: $f_\nu(t) \propto \nu^{-\beta} t^{-\alpha}$. From this expression, we get $\nu^\beta F_\nu \propto t^{-\alpha}$. Then the afterglow light curves at every segment decayed as $\sim t^{-\alpha}$.

The slope of the decay for the afterglow light curves can be calculated by taking points from the flux and time reading of the swift/XRT.

$$\alpha \approx -\frac{\log f_2 - \log f_1}{\log t_2 - \log t_1} \approx \frac{\log f_1 - \log f_2}{\log t_2 - \log t_1} \tag{4.2.1}$$

Using Equ. (4.2.1), the numerical value of temporal decay index of each GRBs are calculated in the first phase or early steep decay phase as:

$$\alpha_1 = \alpha_{050315} \sim \frac{\log(8.67\times10^{-9}\pm1.1\times10^{-9}) - \log(6.01\times10^{-9}\pm8.9\times10^{-10})}{\log(95.97^{+2.6}_{-2.4}) - \log(85.86^{+2.71}_{-2.31})}$$

The slope without error is calculated by taking the value of flux and time reading

without positive and negative error reading.

$$\alpha_1 = \alpha_{050315} \sim 3.3$$

The positive error of the slope is calculated from the positive errors of the flux and time errors of swift/XRT. Then by taking the positive values of flux and time, we got

$$\alpha_1 = \alpha_{050315} \sim 3.22$$

The negative error of the slope is calculated also using negative errors of the data.

$$\alpha_1 = \alpha_{050315} \sim 3.54$$

Finally the slope of the early steep decay slope or the temporal decay index for GRB050315 become

$$\alpha_1 = \alpha_{050315} \sim 3.3^{+0.24}_{-0.08} \tag{4.2.2}$$

Similarly, the decay slope of GRB050505 is also analysed using

$$\alpha_1 = \alpha_{050505} \approx -\frac{\log f_2 - \log f_1}{\log t_2 - \log t_1}$$

$$\alpha_1 = \alpha_{050505} \sim \frac{\log(2.57\times10^{-11}\pm5.7\times10^{-12}) - \log(1.6\times10^{-11}\pm3.4\times10^{-12})}{\log(3498.96^{+73.66}_{-84.3}) - \log(2886.95^{+41.29}_{-53.99})}$$

The value of α_{050505} is found by using the same procedure with α_{050315}.

$$\alpha_1 = \alpha_{050505} \sim 2.6^{+0.06}_{-0.03} \tag{4.2.3}$$

And the next two decay slope of the GRBs are also calculated with the same method and given as

$$\alpha_1 = \alpha_{050724} \sim 5.8^{+0.03}_{-0.2} \tag{4.2.4}$$

$$\alpha_1 = \alpha_{050730} \sim 2.87^{+0.14}_{-0.01} \tag{4.2.5}$$

Considering high latitude emission i.e in early steep decay phase curvature effect is assumed. Then we found the value of spectral index by using $\beta = \alpha - 2$. The spectral values of early steep decay for our samples of GRBs are given bellow:
The numerical values of spectral index for GRB050315, GRB050505, GRB050724 and GRB050730 are calculated from their respective temporal index approximation.

$$\beta_{050315} \approx \alpha_{050315} - 2 \approx 3.3^{+0.24}_{-0.08} - 2$$

Finally we get, the value of spectral index GRB050315 as

$$\beta_{050315} \approx 1.3^{+0.24}_{-0.08} \tag{4.2.6}$$

Using similar procedure,we have the values of GRB050505, GRB050724 and GRB050730 as

$$\beta_{050505} \approx 0.6^{+0.06}_{-0.03} \tag{4.2.7}$$

$$\beta_{050724} \approx 3.8^{+0.03}_{-0.2} \tag{4.2.8}$$

$$\beta_{050730} \approx 0.87^{+0.14}_{-0.01} \tag{4.2.9}$$

According to the above results, when we compared the values of each GRBs, the numerical value of temporal decay index is nearly consistent to the theoretical value

of the afterglow light curves. The value of GRB050315 is exactly consistent with the value of $3 < \alpha_1 < 5$. The numerical value of GRB050724 become largest. This value indicated that it decayed early from a high altitude. In this phase, GRB050724 declined rapidly comparing to the others. However, GRB050505 has slow decaying afterglow light curve segment in phase I.

In this phase, the spectral index is also assumed and calculated with respect to each GRBs. The values of spectral index is the only indicators on this phase. As a light curves' slope increased with time, the flux from higher latitude is took over. For higher latitude the kinetic energy is gradually converted to heat and the afterglow gradually fades and rapidly decayed.

As the temporal decay slope increased, the luminosity of each burst decreased. As we discussed in section (2.5), the luminosity of each burst is $\sim t^{-\alpha_1}$. As the α_1 increased, the the luminosity of afterglow light curves have been died out rapidly. In the early steep decay phase, the isotropic kinetic energy decreased rapidly. Then GRB050724 has been decreased energy rapidly in the early steep decay stage from our samples. Finally, the high kinetic energy in prompt phase is rapidly decreased as the time increased in the early steep decay.

4.2.2 Numerical analysis of temporal indices in phase II

As we have discussed in section (2.4) of this thesis, the numerical value of temporal decay index of shallow decay or plateau phase is $\sim 0.5 - 1.0$. We have used the relation of flux and time for our samples

$$\alpha \approx -\frac{\log f_2 - \log f_1}{\log t_2 - \log t_1}$$

to find the value of α_2 for each GRBs.

We have found the slope without error by taking the value of flux and time reading without positive and negative error reading as:

$$\alpha_2 = \alpha_{050315} \sim 0.54$$

The positive error's of the decay is

$$\alpha_2 = \alpha_{050315} \sim 0.65$$

And the negative error of the decay is ≈ 0.51. The value of the slope of the decay with error measurement is

$$\alpha_2 = \alpha_{050315} \sim 0.54^{+0.11}_{-0.03} \tag{4.2.10}$$

Using the same numerical analysis for GRB050505, GRB050724 and GRB050730, we provide the following decaying slope of these phase.

$$\alpha_2 = \alpha_{050505} \sim 0.79^{+0.01}_{-0.03} \tag{4.2.11}$$

$$\alpha_2 = \alpha_{050724} \sim 0.66^{+0.03}_{-0.1} \tag{4.2.12}$$

$$\alpha_2 = \alpha_{050730} \sim 0.48^{+0.28}_{-0.01} \tag{4.2.13}$$

Theoretically in canonical light curves, the slope of the decay in shallow phase is larger than 0.5 and less than 1.0. This indicated that the value of the temporal decay index in phase II is $0.5 < \alpha_2 < 1.0$. For our samples, the temporal decay slope is consistent with the theoretical value of decay slope of the GRBs afterglow light curves. But the temporal decay index of GRB050730 showed that this high plateau

because the slope is smaller when we compared from others. For these GRBs, there is no spectral evolution across each breaks.

In this phase, energy declines slowly. This indicated that the energy has been transferred slowly from ejecta to the ambient medium [65]. The energy delayed may be due to the reverse shocks. The energy injection from the ejecta was with wide Γ distribution. Generally in this phase, the energy is decayed slowly with a very small decay slope.

4.2.3 Numerical analysis of temporal indices in phase III

The numerical values of the above GRB samples in normal and late steep decay phase were calculated using

$$\alpha \approx -\frac{\log f_2 - \log f_1}{\log t_2 - \log t_1}$$

. The values of the temporal indices in each GRBs are calculated by substituting all the data from table (4.2.). The values provided for each GRBs have been listed below.

$$\alpha_3 = \alpha_{050315} \sim 1.8^{+0.02}_{-0.35} \tag{4.2.14}$$

$$\alpha_3 = \alpha_{050505} \sim 2.4^{+0.07}_{-0.42} \tag{4.2.15}$$

$$\alpha_3 = \alpha_{050724} \sim 1.5^{+0.21}_{-0.13} \tag{4.2.16}$$

$$\alpha_3 = \alpha_{050730} \sim 1.3^{+0.01}_{-0.02} \tag{4.2.17}$$

This phase, as we have discussed in section (2.4), is called the late steep decay for GRBs which have two breaks. GRB050515 and GRB050505 have two breaks and

they have late steep decay slope. As we have shown on the above Fig. (4.1) and Fig. (4.2), the slopes of the GRBs have been greater than the shallow decay which it indicated high energy decreasing process. The luminosity of the GRBs have been reduced rapidly. For the two GRBs, this phase was the final decay that the energy died out throughout.

So that when we compared the temporal decay index, the first two GRBs were nearly consistent to the theoretical prediction of α_3. In late steep decay, the afterglow light curves decayed greater than $\sim t^{-2}$. The late steep decay slope what have found was $\alpha_3 = \alpha_{050315} \sim 1.8^{+0.02}_{-0.35}$ and $\alpha_3 = \alpha_{050505} \sim 2.4^{+0.07}_{-0.42}$. This indicated that the numerical value of late steep decay slope was nearly $\alpha_3 > 2$. The results of this thesis showed that GRB050315 and GRB050505 nearly confirmed to the prediction. GRB050505 declined rapidly and GRB050315 was slowed relative to GRB050505.

However, GRB050724 and GRB050730 have three breaks. For the two GRBs this phase is called normal decay phase. For a normal decay phase in standard forward shock, the temporal decay slope is $1.0 < \alpha_3 < 1.5$. In this phase, the luminosity of of the GRBs was decreased with the $\sim t^{-\alpha_3}$ in which the values of decay slope was $\alpha_3 = \alpha_{050724} \sim 1.5^{+0.21}_{-0.13}$ and $\alpha_3 = \alpha_{050730} \sim 1.3^{+0.01}_{-0.02}$. The energy decaying was rapid comparing to the shallow decay in bath of the GRBs. GRB050724 and GRB050730 showed normal decay relatively near to $1.0 < \alpha_3 < 1.5$. Here, GRB050724 declined early since the slope was greater than GRB050730.

4.2.4 Numerical analysis of temporal indices in phase IV

This phase is the late steep phase in which jet become declined. The GRBs that have late steep decay phase from my samples were GRB050724 and GRB050730. These GRBs were steep decayed means they have temporal decay index of greater than 2.

The numerical value of temporal decay slope provided to the two GRBs were analyzed as follow by using

$$\alpha \approx -\frac{\log f_2 - \log f_1}{\log t_2 - \log t_1}$$

.

$$\alpha_4 = \alpha_{050724} \sim 3.1^{+0.1}_{-0.25} \tag{4.2.18}$$

$$\alpha_4 = \alpha_{050730} \sim 2.6^{+0.35}_{-0.23} \tag{4.2.19}$$

From our data only GRB050724 and GRB050730 have three breaking time. The numerical value which is provided was consistent to the theoretical numerical value. This means they decayed rapidly after normal emission. The luminosity of the two GRBs has a decay power law $\sim t^{-\alpha_4}$ with the value of $\alpha_4 = \alpha_{050724} \sim 3.1^{+0.1}_{-0.25}$ and $\alpha_4 = \alpha_{050730} \sim 2.6^{+0.35}_{-0.23}$. The energy has been died out as the time increased and the energy totally have decreased in related to the respective decay slope.

In summary, the numerically calculated values of the sampled data were nearly consistent to their respective theoretical values in each phase and the energy decaying has been occurred in each phase. The above result can be summarized as

slope	theoretical value	GRB050315	GRB050505	GRB050724	GRB050730
α_1	3 - 5	$\sim 3.3^{+0.24}_{-0.08}$	$\sim 2.6^{+0.06}_{-0.03}$	$\sim 5.8^{+0.03}_{-0.2}$	$\sim 2.87^{+0.14}_{-0.01}$
α_2	0.5 - 1.0	$\sim 0.54^{+0.11}_{-0.03}$	$\sim 0.79^{+0.01}_{-0.03}$	$\sim 0.66^{+0.03}_{-0.1}$	$\sim 0.48^{+0.28}_{-0.01}$
α_3	1.0 - 1.5	$\sim 1.8^{+0.02}_{-0.35}$	$\sim 2.4^{+0.07}_{-0.42}$	$\sim 1.5^{+0.21}_{-0.13}$	$\sim 1.3^{+0.01}_{-0.02}$
α_4	> 2	-	-	$\sim 3.1^{+0.1}_{-0.25}$	$\sim 2.6^{+0.35}_{-0.23}$

Table 4.3: Result summary of temporal decay index

Chapter 5

Conclusion

In this thesis, swift afterglow light curves have been analyzed. The concept of afterglow light curves were very difficult to understand before swift. However, the long lived afterglows observed at low energies are believed to be produced by photon electrons excited in the external shock arising from the interaction between the relativistic outflows and the surrounding at $r \approx 10^{16} - 10^{18}$ cm from the source. In afterglow theory, the light curves represented the way of energy dissipation in different stages of emission.

We have presented X-ray light curves for four GRB_s monitored by swift from January 2005 - July 2005. These light curves mostly started decaying as early as $\lesssim 10^2$ s after the GRB trigger. The most striking result we obtained is that the decay slope for the early steep decay X-ray light curves nearly in $3 \lesssim \alpha_1 \lesssim 5$ and the energy decaying process has been decreased rapidly. All the values of temporal index in our sample were nearly consistent with the basic temporal approximation of canonical light curves of initial steep decay. The temporal and spectral indices are the main important factors for light curves in afterglow physics.

In afterglow physics, the canonical x-ray afterglow pictures represent the initial

steep decay $F_x \sim t^{-\alpha_1}$ with a temporal index $3 \lesssim \alpha \lesssim 5$ and an energy spectrum $F_\nu \sim \nu^{-\beta}$ with an energy spectral index $1 \lesssim \beta_1 \lesssim 2$ in the time interval bellow the break time. Then afterglow light curves rapidly decayed and an important values were in the region of theoretical predicted numerical values. Since the flux decay and the time reading in the X-ray were error oriented, except GRB050315, the rest of GRBs weren't exactly fit to the actual value.

All GRBs in our sample were consistent to the numerical value of the slope of canonical light curves in plateau phase. Since the temporal decay index in the shallow phase is between 0.5 and 1.0, our result for all samples were between this boundary. When the energy is terminated, the decay of light curves become slow down and the transition to phase three (normal decay) is occurred. Generally in this phase all the GRBs slowed down.

When we considered phase three of afterglow light curves of our samples, they are grouped into two. For GRB050315 and GRB050505, this stage were their late steep decay phase. Then, the numerical values of temporal decay index were near to above two i.e consistent to the accepted values of the canonical afterglow light curves. However, GRB050724 and GRB050730 had three break points of time and then they were in normal decay phase in which their decay slope have been valid.

The last phase were late steep decay phase. GRB050724 and GRB050730 showed the situation fading in this light curve segment. GRB050724 decayed more rapidly than GRB050730 that means the energy become slow down quickly.

Generally in this thesis, we have calculated numerical value of the temporal decay index of the the four phases of afterglow light curves. And our results of four $GRBs'$ indices were nearly consistent with the expected value.

At last, it is possible to estimate the temporal decay slope from random data of energy flux and time on each segments of afterglow light curves and the accuracy of the values are the problem to be studied for researchers.

Bibliography

[1] *The American Heritage Stedman's Medical Dictionary* ,1995 by Houghton's Mifflin Campany.

[2] Tilan N.Ukwatta , *Spectral Lags and Variability of Gamma-Ray Burst in Swift Era* , 2010, George Washington, America, P. 1-2.

[3] Costa E., Frontera F., Heise J., et al., *Discovery of an X-ray afterglow associated with the Gamma-ray burst of 28 February 1997*, 1997, Nature, 387, 783

[4] Rhoads, J. E. *The Dynamics and Light Curves of Beamed Gamma-Ray Burst Afterglows*. ApJ 525, 737-749, (1999).

[5] Rees, M. J. and Meszaros, P. *Refreshed Shocks and Afterglow Longevity in Gamma-Ray Bursts* ApJ 496, L1-L5, (1998).

[6] Rhoads, J. E., Sep. 1997. *How to Tell a Jet from a Balloon: A Proposed Test for Beaming in Gamma-Ray Bursts*. ApJ487, L1L4.

[7] Holland, S. T. et al. *Optical Photometry of GRB021004*: The First Month. AJ, 125, 2291-2298, (2003).

[8] Kumar, P., Panaitescu, A., Sep. 2000. *Steepening of Afterglow Decay for Jets Interacting with Stratified Media*. ApJ541, L9L12.

[9] Klebesadel R., W., Strong I., B., Olson R., A., 1973, *Observations of GammaRay Bursts of Cosmic Origin*, 1968, ApJ, 182, L85

[10] Meegan C. A., Fishman G. J., Wilson R. B., Horack J. M., Brock M. N., Paciesas W. S. Pendleton G. N., Kouveliotou C., *Spatial distribution of gammaray bursts observed by BATSE*, 1992,Nature, 355, 143

[11] Briggs, M. S., Paciesas, W. S., Pendleton, G. N. et al. 1996, *Gamma-Ray Bursts: 3rd Huntsville Symposium* (AIP Conf. Proc. 385), ed.

[12] S. Mallozzi. *BATSE Web* - http://f64.nsstc.nasa.gov. 2010.

[13] Boella, et al. *BeppoSAX, the wide band mission for X-ray astronomy.* Astron. Astrophys. Suppl. Ser., 122(2):299, 1997.

[14] Costa, F. Frontera, J. Heise, et al. *Discovery of an X-ray afterglow associated with the Gamma-ray burst on 28 February 1997.* Nature, 387:783785, June 1997b.

[15] Van Paradijs, J., et al., Apr. 1997. *Transient optical emission from the error box of the -ray burst of 28 February 1997.* Nature386, 686689.

[16] Frail D. A., Kulkarni S. R., Nicastro L., Feroci M., Taylor G. B., *The radio afterglow from the γ-ray burst of 8 May 1997*, 1997, Nature, 389, 261

[17] Bloom J. S., Kulkarni S. R., Harrison F., Prince T., Phinney E. S., Frail D. A., *Expected Characteristics of the Subclass of Supernova GammaRay Bursts*, 1998, ApJ, 506, L105

[18] J.D. Myers (September 26, 2007). *"Swift Guest Investigator Program Frequently Asked Questions"*. NASA/GSFC. Retrieved May 2, 2009.

[19] J.D. Myers (February 28, 2006). *"Swift's Burst Alert Telescope (BAT)"*. NASA/ GSFC. Retrieved May 2, 2009.

[20] J.D. Myers (August 15, 2008). *"Swift's X-Ray Telescope (XRT)"*. NASA/ GSFC. Retrieved May 2, 2009.

[21] J.D. Myers (December 14, 2006). *"Swift's Ultraviolet/Optical Telescope (UVOT)"*. NASA / GSFC. Retrieved May 2, 2009

[22] Gehrels, N. et al. *The Swift Gamma-Ray BurstMission*. ApJ 611, 1005-1020, (2004).

[23] David Whitehouse (May 11, 2005). *"Blast hints at black hole birth"*. BBC News. Retrieved July 12, 2011.

[24] Reddy, Francis (April 19, 2010). *"NASA's Swift Catches 500th Gamma-ray Burst"*. NASA. Retrieved October 10, 2016.

[25] "*Swift GRB Table Stats*". NASA. Archived from the original on November 10, 2013. Retrieved November 10, 2013.

[26] Reddy, Francis (November 6, 2015). *"NASA's Swift Spots its Thousandth Gamma-ray Burst"*. NASA. Retrieved October 10, 2016.

[27] Kouveliotou C., Meegan C. A., Fishman G. J., Bhat N. P., Briggs M. S., Koshut T. M., Paciesas W. S., Pendleton G. N., *Identification of two classes of gammaray bursts*, 1993, ApJ, 413,L101

[28] Barthelmy, S. D. et al. 2005 GRB 050724, *A short hard burst with a lot of features*. Nature 438,994996. (doi:10.1038/nature04392)

[29] Burrows, D. N. et al. 2005 *Bright X-ray flares in gamma-ray burst afterglows*. Science 309, 1833.(doi:10.1126/science.1116168)

[30] Cavallo, M.J. Rees, *A qualitative study of cosmic fireballs and gamma-ray bursts*.Mon. Not. R. Astron. Soc. 183, 359365 (1978)

[31] Meszaros, M.J. Rees, *Gamma-Ray Bursts*. ArXiv e-prints (2014)

[32] Meszaros, P. and Rees, M. J. (1993). *Relativistic fireballs and their impact on external matter - Models for cosmological gamma-ray bursts*. ApJ., 405:278/284.

[33] C. Thompson, P. Meszaros, M. J. Rees. *Thermalization in Relativistic Outflows and the Correlation between Spectral Hardness and Apparent Luminosity in Gamma-Ray Bursts*. ApJ 666 (2007) 10121023.

[34] Gomboc. *Unveiling the Secrets of Gamma-Ray Bursts*. arXiv:astro-ph/1206.3127, 2012.

[35] Rees, P. Meszaros, *Unsteady outflow models for cosmological gamma-ray bursts*. Astrophys. J. 430, 9396 (1994). doi:10.1086/187446

[36] Beloborodov, A. M. *On the Efficiency of InternalShocks in Gamma-Ray Bursts*. ApJ 539, L25- L28, (2000).

[37] Kobayashi, S. and Sari, R. *Ultraefficient Internal Shocks.* ApJ 551, 934-939, (2001).

[38] Meszaros, M.J. Rees, *Tidal heating and mass loss in neutron star binaries - Implications for gamma-ray burst models*. Astrophys. J. 397, 570575 (1992). doi:10.1086/171813.

[39] Meszaros, P., Rees, M. J. *Optical and Long- Wavelength Afterglow from Gamma-Ray Bursts*, ApJ 476, 232-237, (1997).

[40] Vedrenne, G. and Atteia, J. (2010). Gamma-Ray Bursts.

[41] Wijers, R. A. M. J., Rees, M. J., Meszaros, P., Jul. 1997. *Shocked by GRB970228: the afterglow of a cosmological Fireball*. MNRAS 288, L51 L56.

[42] Harrison et al 1999. *Optical and Radio Observations of the Afterglow from GRB 990510: Evidence for a Jet*. ApJ 523, L121 L124.

[43] Frail et al Jul. 2000. A 450 *Day Light Curve of the Radio Afterglow of GRB 970508: Fireball Calorimetry*. ApJ 537,191204.

[44] Wijers, R. A. M. J., Galama, T. J., Sep. 1999. *Physical Parameters of GRB970508 and GRB 971214 from Their Afterglow Synchrotron Emission*. ApJ 523, 177 186.

[45] Zhang, B., Dec. 2006. Astrophysics: *A burst of new ideas*. Nature 444, 1010 1011.

[46] Nousek et al ,May 2006. *Evidence for a Canonical Gamma-Ray Burst Afterglow Light Curve in the Swift XRT Data*. ApJ 642, 389 400.

[47] Dermer, C. D., Mitman, K. E., Mar. 1999. *Short-Timescale Variability in the External Shock Model of Gamma-Ray Bursts*. ApJ 513, L5 L8.

[48] Dermer, C. D., Oct. 2004. *Curvature Effects in Gamma-Ray Burst Colliding Shells*. ApJ 614, 284 292.

[49] Fan, Y. Z., Wei, D. M., Nov. 2005. *Late internal-shock model for bright X-ray flares in gamma-ray burst afterglows and GRB* 011121. MNRAS 364, L42 L46.

[50] Genet, F., Granot, J., Nov. 2009. *Realistic analytic model for the prompt and high-latitude emission in GRBs*. MNRAS 399, 1328 1346.

[51] Fan, Y., Piran, T., Jun. 2006b. *Gamma-ray burst efficiency and possible physical processes shaping the early afterglow*. MNRAS 369, 197 206.

[52] Mangano et al, Jan. 2007. *Swift XRT Observations of the Afterglow of XRF* 050416A. ApJ 654, 403 412.

[53] Ramirez-Ruiz, E., Dray, L. M., Madau, P., Tout, C. A., Nov. 2001. *Winds from massive stars: implications for the afterglows of Gamma-Ray bursts*. MNRAS 327, 829 840

[54] Birnbaum, May 2012. *Observational constraints on the external shock prior emission hypothesis of Gamma-Ray bursts*. MNRAS 422, 393 400.

[55] Chevalier, R. A., Li, Z.-Y., Jun. 2000. *Wind Interaction Models for Gamma-Ray Burst Afterglows: The Case for Two Types of Progenitors*. ApJ 536,195 212.

[56] Granot, J., Sari, R., Apr. 2002. *The Shape of Spectral Breaks in Gamma-Ray Burst Afterglows*. ApJ 568, 820 829.

[57] Ghisellini, Apr. 2007. "*Late Prompt" Emission in Gamma-Ray Bursts?* ApJ 658, L75 L78.

[58] Linder, Apr. 2010. *Collapsar Accretion and the Gamma-Ray Burst X-Ray Light Curve*. ApJ 713,800 815.

[59] Sari, R., Narayan, R., Piran, T., Dec. 1996. *Cooling Timescales and Temporal Structure of Gamma-Ray Bursts*. ApJ 473, 204.

[60] Sari, R., Piran, T., Narayan, R., Apr. 1998. *Spectra and Light Curves of Gamma-Ray Burst Afterglows*. ApJ 497, L17+.

[61] Fenimore et al, Aug. 1995. *Gamma-Ray Burst Peak Duration as a Function of Energy*. ApJ 448, L101+.

[62] Nousek, J. A., et al. 2005, ApJ, submitted (*astro-ph*/0508332).

[63] http://www. swift. ac. uk/xrt.curves/

[64] Evans et al, Aug. 2009. *Methods and results of an automatic analysis of a complete sample of Swift-XRT observations of GRBs*. MNRAS 397, 1177 1201.

[65] Kobayashi, S. and Zhang, B. The Onset of Gamma-Ray Burst Afterglow. ApJ, in press (astro-ph/0608132) (2006).

Declaration

This thesis is my original work, has not been presented for a degree in any other University and that all the sources of material used for the thesis have been duly acknowledged.

Name: Deres Endalamaw Ayele

Signature:

Place and time of submission: Addis Ababa University, October, 2017.

This thesis has been submitted for examination with my approval as University advisor.

Name: Dr. Remudin Reshid

Signature: